Atmos. Chem. Phys. Discuss., 14, 5535–5560, 2014
www.atmos-chem-phys-discuss.net/14/5535/2014/
doi:10.5194/acpd-14-5535-2014

Atmospheric Chemistry and Physics Discussions

Atmospheric photochemistry of aromatic hydrocarbons: OH budgets during SAPHIR chamber experiments

S. Nehr[1,*], B. Bohn[1], H.-P. Dorn[1], H. Fuchs[1], R. Häseler[1], A. Hofzumahaus[1], X. Li[1], F. Rohrer[1], R. Tillmann[1], and A. Wahner[1]

[1]Institut für Energie- und Klimaforschung, IEK-8: Troposphäre, Forschungszentrum Jülich GmbH, Jülich, Germany
[*]now at: Verein Deutscher Ingenieure e.V., Kommission Reinhaltung der Luft, Düsseldorf, Germany

Received: 28 January 2014 – Accepted: 23 February 2014 – Published: 3 March 2014

Correspondence to: B. Bohn (b.bohn@fz-juelich.de)

Published by Copernicus Publications on behalf of the European Geosciences Union.

Abstract

Current photochemical models developed to simulate the atmospheric degradation of aromatic hydrocarbons tend to underestimate OH radical concentrations. In order to analyse OH budgets, we performed experiments with benzene, toluene, *p*-xylene, and 1,3,5-trimethylbenzene in the atmosphere simulation chamber SAPHIR. Experiments were conducted under low-NO conditions (typically 0.1–0.2 ppb) and high-NO conditions (typically 7–8 ppb), and starting concentrations of 6–250 ppb of aromatics, dependent on OH rate constants. For the OH budget analysis a steady-state approach was applied where OH production and destruction rates (P_{OH} and D_{OH}) have to be equal. The P_{OH} were determined from measurements of HO_2, NO, HONO, and O_3 concentrations, considering OH formation by photolysis and recycling from HO_2. The D_{OH} were calculated from measurements of the OH concentrations and total OH reactivities. The OH budgets were determined from D_{OH}/P_{OH} ratios. The accuracy and reproducibility of the approach were assessed in several experiments using CO as a reference compound where an average ratio $D_{OH}/P_{OH} = 1.13 \pm 0.19$ was obtained. In experiments with aromatics, these ratios ranged within 1.1–1.6 under low-NO conditions and 0.9–1.2 under high-NO conditions. The results indicate that OH budgets during photo-oxidation experiments with aromatics are balanced within experimental accuracies. Inclusion of a further, recently proposed OH production via $HO_2 + RO_2$ reactions led to improvements under low-NO conditions but the differences were small and insignificant within the experimental errors.

1 Introduction

Large amounts of volatile organic compounds (VOCs) are released into the earth's atmosphere from both biogenic and anthropogenic sources with an estimated global emission rate on the order of 10^{12} kg year^{-1} (Piccot et al., 1992; Arneth et al., 2011). Aromatic hydrocarbons like benzene, toluene, xylenes, and trimethylbenzenes are

ACPD
14, 5535–5560, 2014

among the most abundant organic trace constituents observed in the urban environment (Fortin et al., 2005; Johnson et al., 2010). Major emission sources of aromatics are vehicle exhaust, solvent usage, and residential wood burning (Hawthorne et al., 1988; Niedojadlo et al., 2007). Once emitted to the atmosphere, organic compounds are oxidized photochemically and are then removed by wet or dry deposition.

The self-cleaning ability of the atmosphere mainly results from the presence of OH radicals that initiate the oxidation processes of most VOCs, including aromatics (Ehhalt, 1999). The predominant primary atmospheric OH source is the photolysis of O_3 (Finlayson-Pitts and Pitts, 2000). At wavelengths below about 330 nm O_3 is photolysed to electronically excited $O(^1D)$ that subsequently may react with water vapour to give OH.

$$O_3 + h\nu \rightarrow O(^1D) + O_2 \quad \lambda < 330\,\text{nm} \tag{R1}$$

$$O(^1D) + H_2O \rightarrow 2OH \tag{R2}$$

Only a minor fraction of $O(^1D)$ reacts with H_2O, the remainder is deactivated by collisional quenching followed by a regeneration of O_3. Photolysis of HONO at wavelengths below about 400 nm is another important OH source, especially close to the ground and in the morning hours (Kleffmann, 2007), but also in simulation chambers like SAPHIR (Rohrer et al., 2005).

$$HONO + h\nu \rightarrow OH + NO \quad \lambda < 400\,\text{nm} \tag{R3}$$

These primary photolytic production processes are necessary but insufficient to maintain an effectual OH concentration, especially in the presence of high concentrations of VOCs. A regeneration of OH from HO_2 radicals is therefore essential:

$$HO_2 + NO \rightarrow OH + NO_2 \tag{R4}$$

$$HO_2 + O_3 \rightarrow OH + 2O_2 \tag{R5}$$

HO_2 can be formed photolytically (e.g. from formaldehyde), directly following the initial OH + VOC reactions (prompt HO_2), or indirectly from organic peroxy radicals (RO_2)

ACPD
14, 5535–5560, 2014

after another reaction step involving NO:

$$OH + VOC \rightarrow RO_2 \quad \text{(R6)}$$

$$RO_2 + NO \rightarrow RO + NO_2 \quad \text{(R7)}$$

$$RO + O_2 \rightarrow R'O + HO_2 \quad \text{(R8)}$$

Thus, the presence of NO leads to a propagation of the radical chain and counteracts terminating HO_2 and RO_2 self- and cross-reactions. NO itself is regenerated during daylight by NO_2 photolysis that is accompanied by a net O_3 production. Typically the NO Reaction (R4) is dominating while the O_3 Reaction (R5) is of minor importance because of a very small rate constant. However, at too high concentrations of NO_x, OH concentrations decrease because of a terminating $OH + NO_2$ reaction.

In contrast to this concept, recent field studies in areas characterized by high biogenic VOC and low NO concentrations revealed unexpectedly high levels of OH that could not be explained by model calculations. It was speculated that these discrepancies are explainable by so far unaccounted OH recycling processes, e.g. OH formation via $RO_2 + HO_2$ reactions (Lelieveld et al., 2008), unimolecular decomposition reactions of RO_2 radicals (Peeters et al., 2009; Crounse et al., 2011; Fuchs et al., 2013) and/or fast photolysis of hydroperoxide compounds (Wolfe et al., 2012). Alternatively, a generic mechanism assuming the presence of an unknown compound acting chemically similar as NO was postulated and utilized to quantify the missing rate of OH recycling (Hofzumahaus et al., 2009). Based on a steady-state approach for OH, Hofzumahaus et al. (2009) compared the known production and destruction rates of OH by taking measured concentrations of OH, HO_2, NO and the total OH reactivity of ambient air. It was concluded that during a field campaign in the Pearl River Delta in southern China, the conventional OH recycling rate by $HO_2 + NO$ was too small by a factor of three to explain the measured OH under low-NO conditions (Hofzumahaus et al., 2009; Lu et al., 2012).

In this work, a similar, widely model-independent approach to investigate OH budgets is used for the analysis of SAPHIR simulation chamber experiments with aromatic

ACPD
14, 5535–5560, 2014

compounds. Aromatics contributed significantly to the OH reactivity during the measurements in the Pearl River Delta (Lou et al., 2010) and potential additional OH recycling from aromatics oxidation would therefore impact the OH budget. Previous chamber experiments with aromatics indeed showed unexpectedly high OH concentrations compared to model calculations (Bloss et al., 2005a). Moreover, recent laboratory work revealed high yields of prompt HO_2 (Nehr et al., 2011, 2012) and effective OH recycling in reactions of HO_2 with aromatics-related peroxy radicals (Birdsall et al., 2010; Birdsall and Elrod, 2011):

$$RO_2 + HO_2 \rightarrow RO + O_2 + OH \quad \text{(R9)}$$

An OH budget investigation under the controlled conditions in SAPHIR was therefore performed with four selected monoaromatic compounds together with reference experiments with CO to evaluate the validity and the accuracy of the approach.

2 Experimental

The outdoor atmosphere simulation chamber SAPHIR at Forschungszentrum Jülich facilitates the investigation of photochemical processes under defined conditions (cf. Karl et al., 2004; Poppe et al., 2007). The SAPHIR chamber has a cylindrical shape (18 m length, 5 m diameter, 270 m^3 volume). The chamber wall is a Teflon film that is held by a steel frame. The teflon film is chemically inert and transmits solar radiation without significant absorption (Bohn and Zilken, 2005). A shutter system allows for a rapid opening and closing of the chamber roof within about 60 s.

2.1 Analytical instrumentation

SAPHIR is equipped with a comprehensive set of analytical instruments. Measurements of experimental boundary conditions include temperature (ultrasonic anemometer), pressure (capacitive gauge), replenishment flow rate (mass flow controller), and

ACPD
14, 5535–5560, 2014

photolysis frequencies (spectroradiometer). Measurements of trace gas concentrations include volatile organic compounds (proton transfer reaction time of flight mass spectrometry, PTR-TOF-MS), HCHO (Hantzsch reaction), HONO (long path absorption photometry, LOPAP), CO (reduction gas analysis, RGA), CO_2, CH_4, H_2O (cavity ring-down spectroscopy, CRDS), as well as NO, NO_2, and O_3 (chemiluminescence, CL). The reader is referred to previous publications for detailed information on the analytical instrumentation of SAPHIR (Wegener et al., 2007; Fuchs et al., 2010, 2012; Dorn et al., 2013; Fuchs et al., 2013, and references therein).

Table 1 provides an overview of the key instruments for this study and their performances. Briefly, the detection of OH, HO_x (sum of OH and HO_2), and RO_x (sum of OH, HO_2 and RO_2) was performed by laser-induced fluorescence (LIF) spectroscopy (Holland et al., 2003; Fuchs et al., 2008, 2011). From these measurements, concentrations of HO_2 and RO_2 radicals were determined. Moreover, differential optical absorption spectroscopy (DOAS) (Dorn et al., 1995; Schlosser et al., 2007, 2009) was employed for the measurement of OH radical concentrations.

The total OH reactivity k_{OH}, which is equivalent to the inverse atmospheric OH lifetime, was measured by the flash photolysis/laser-induced fluorescence (FP/LIF) technique that was first realized by Calpini et al. (1999) and later by Sadanaga et al. (2004). k_{OH} is a pseudo-first-order rate constant given by the following expression:

$$k_{OH} = \sum_i k_{X_i+OH}[X_i] \quad (1)$$

$[X_i]$ denotes the concentration of a reactive trace constituent and k_{X_i+OH} is the respective second-order rate constant. The instrument used in this work at SAPHIR was deployed in previous field campaigns and was described in detail elsewhere (Hofzumahaus et al., 2009; Lou et al., 2010).

ACPD
14, 5535–5560, 2014

2.2 Materials

The SAPHIR chamber was operated with highly purified synthetic air made from liquid N_2 and O_2 (99.9999 %, Linde). Benzene (99.8 %, Merck), toluene (99.9 %, Merck), *p*-xylene (99.8 %, BDH Prolabo), and 1,3,5-trimethylbenzene (1,3,5-TMB; 99.0 %, Sigma Aldrich) were used as purchased. For experiments with elevated NO concentrations a mixture of 600 ppm of NO (99.5 %, Messer Griesheim) in N_2 (99.999 %) was added to the chamber. CO was used in pure form (99.997 %, Messer Griesheim). Gases were introduced into the chamber using calibrated mass flow controllers. Liquids were injected by microliter syringes via a heated injection port.

2.3 Experiment procedure

The sequence of a typical SAPHIR experiment is shown in Fig. 1 taking the photooxidation of 1,3,5-TMB performed on 17 June 2010 as an example. All experiments started after the chamber was flushed overnight with high purity dry synthetic air to purge trace gases below the limits of detection. A fan was used to assure homogeneous mixing. In the morning, the clean chamber was humidified by flushing ultrapure water vapour (Milli-Q) from a vaporizer with a high flow of zero air into the chamber. Afterwards, the shutter system was opened and the chamber was exposed to sunlight. Usually, no other trace gases were then added for a period of about two hours. During this so-called zero air period, HONO was formed photolytically at the chamber walls dependent on humidity and UV radiation (Rohrer et al., 2005). Relative humidities were around 40 % during the illumination periods. Photolysis of HONO is the major primary source of OH radicals in SAPHIR and therefore OH (and NO) concentrations were found to increase during this period. Moreover, the background OH reactivity that typically builds up within SAPHIR without addition of any reactants, slowly rose to about $2\,s^{-1}$. Subsequently, the compound of interest (CO or an aromatic hydrocarbon) was injected into the chamber. The example in Fig. 1 shows an injection of about 6 ppb of 1,3,5-TMB as reproduced by PTR-TOF-MS and the OH reactivity instrument. The

ACPD
14, 5535–5560, 2014

resulting concentration of OH radicals in SAPHIR depended on the concentrations of OH reactants and was further modulated by solar radiation. The initial aromatics concentrations were chosen dependent on the OH + aromatics rate constants to result in starting OH reactivities of about 10 s^{-1}. This ensured that the total reactivity was dominated by the aromatic compound while it was still low enough to allow the detection of OH at good signal-to-noise ratios. After 6–8 h of illumination the chamber shutter system was closed. Experiments with aromatics were performed under low-NO (typically 0.1–0.2 ppb after injection of aromatics) and high-NO (7–8 ppb) conditions. In the case of high-NO experiments, NO was injected 30 min prior to the addition of the aromatic. For low-NO experiments the source of NO was photolysis of HONO. Table 2 provides an overview of all SAPHIR experiments with aromatics utilized in this work.

3 Data analysis and results

The OH production rate P_{OH} resulting from Reactions (R1)–(R5) is given by the following equation.

$$P_{OH} = j_{O(^1D)}[O_3] \times 2c_{OH} + j_{HONO}[HONO] + k_4[HO_2][NO] + k_5[HO_2][O_3] \quad (2)$$

$j_{O(^1D)}$ and j_{HONO} are the photolysis frequencies of Reactions (R1) and (R3), respectively. c_{OH} denotes the fraction of $O(^1D)$ that reacts with H_2O according to Reaction (R2). For the calculation of P_{OH} measured $j_{O(^1D)}$ and j_{HONO} were used and rate constants k_4 and k_5 from recent recommendations: $k_4 = 3.45 \times 10^{-12}\,cm^3\,s^{-1} \times \exp(270\,K/T)$, $k_5 = 2.03 \times 10^{-16}\,cm^3\,s^{-1} \times (T/300\,K)^{4.57} \times \exp(693\,K/T)$ (IUPAC, 2013). The c_{OH} typically were around 0.1 and were calculated using measured water vapour concentrations and recommend rate constants of $O(^1D)$ reactions (IUPAC, 2013).

It turned out that under all conditions P_{OH} was dominated by the NO Reaction (R4). The second most important OH source was photolysis of HONO, the contribution of which is shown in the lower panel of Fig. 1 as an example. It should be noted that in

ACPD
14, 5535–5560, 2014

some experiments where HONO measurements were not available (Table 2) its concentration was estimated from the resulting OH concentration during the zero air period based on a parametrization of the HONO production rate in the chamber (Rohrer et al., 2005). Compared to HONO photolysis, OH production rates by O_3 photolysis and the O_3 Reaction (R5) are almost negligible under the experimental conditions employed, i.e. [O_3]< 20 ppb) (< 50 ppb for some CO experiments).

The OH destruction rate D_{OH} is given by the product of the total OH reactivity and the OH concentration.

$$D_{OH} = k_{OH}[OH] \quad (3)$$

D_{OH} can be calculated from only two measurements because all chemical OH losses are accounted for by the measurements of k_{OH}. In contrast, unaccounted OH recycling processes and/or primary OH sources might be missed in P_{OH} calculated by Eq. (2). In any case, for a short-lived species like OH, the steady-state approximation applies under the conditions of SAPHIR experiments:

$$\frac{\mathrm{d[OH]}}{\mathrm{d}t} = P_{OH} - D_{OH} \approx 0 \quad (4)$$

Thus, ideally also the calculated P_{OH} of Eq. (2) should be balanced by D_{OH}. This analysis is independent of mechanistic details and model simulations. The only exception are the HO_2 data that were corrected for interferences caused by specific organic peroxy radicals (Nehr et al., 2011; Fuchs et al., 2011). However, these corrections were minor, < 20 % in 2010 and < 5 % in 2011, after technical modifications of the LIF instrument that were made before the 2011 experiments (Fuchs et al., 2011). More details on this correction can be found in the Appendix.

The closure of the OH budget was investigated by consulting mean D_{OH}/P_{OH} ratios and their standard deviations for the different experiments. For this, all experimental data were synchronized to the time grid of the instrument with the lowest time resolution (either the OH reactivity instrument during experiments in 2010 or the DOAS instrument

ACPD
14, 5535–5560, 2014

during experiments in 2011). For the calculation of the mean ratios, data points were weighted according to the errors for D_{OH} and P_{OH} resulting from contributions of all measured quantities using error propagation (Table 1).

A total of 13 experiments performed with CO in 2010 and 2011 were evaluated as reference experiments. Some of these experiments were dedicated to investigations of compounds other than aromatics where after an about two-hour CO reference period the compound of interest was injected. In these cases only the CO periods were taken into account. In other experiments several injections of CO were made to cover a wider range of k_{OH}. The average of the mean ratios D_{OH}/P_{OH} obtained in these reference experiments was 1.13 ± 0.19. The 0.13 deviation from unity reflects the accuracy of the experimental approach. This deviation is well within the accuracy of the experimental input data and consequently the OH budget was closed for the CO experiments. The standard deviation of ±0.19 reflects the reproducibility of single experiments.

The results obtained with the different aromatic compounds are listed in Table 3 and examples of plots of D_{OH} as a function of P_{OH} under low- and high-NO conditions are shown in Fig. 2. The mean ratios D_{OH}/P_{OH} ranged between 0.9 and 1.6 and were again mostly greater than unity. No trend was observed for the homologous series of aromatic compounds but low-NO experiments tended to give greater ratios (1.1–1.6) than high-NO experiments (0.9–1.2). Overall, considering the result of the CO reference experiments and experimental errors, OH budgets for all aromatics compounds are regarded as closed.

In order to test the potential influence of the recently proposed OH recycling by Reaction (R9), Eq. (2) was extended accordingly.

$$P^{*}_{OH} = P_{OH} + k_9[HO_2][RO_2] \quad (5)$$

Estimates of the rate constant of Reaction (R9) were taken from the literature ($k_9 = 1 \times 10^{-11}$ cm^3 s^{-1}, Birdsall et al., 2010). Because the RO_2 measurements cannot distinguish between different species, the measured total RO_2 concentrations were used for the calculations. Inclusion of the additional term in Eq. (5) led to somewhat smaller

ACPD
14, 5535–5560, 2014

ratios in particular under low-NO conditions (see right hand side of Table 3 for a direct comparison). However, overall the differences between P^*_{OH} and P_{OH} were small and merely in the range of experimental errors.

4 Discussion

The results listed in Table 3 show that the OH budgets during the OH-initiated degradations of aromatic compounds were reasonably balanced within experimental errors for all investigated compounds. No clear trend was observed in the OH budget analysis for the homologous series of aromatic compounds. Although the degradation mechanism of all aromatics is similar, this result is noteworthy. Because the OH rate constants increase with the degree of methylation (Calvert et al., 2002), the employed initial concentrations of aromatics were very different, e.g. about 250 ppb of benzene and 6 ppb of 1,3,5-TMB. Accordingly, the fractions of the aromatics that were degraded at the end of the experiments differed strongly. While 1,3,5-TMB was completely consumed and k_{OH} decreased monotonically during the course of the experiment, this was not the case for benzene where only a minor fraction was lost and k_{OH} even increased because of more reactive secondary products. Despite these differences, in the temporal evolution of the experiments, no differences in the OH budgets analyses were found. This implies that the results apply in the presence of primary and secondary OH reactants that emerge in aromatic degradation processes.

All results presented in Table 3 are based on OH LIF data that were available in 2010 and 2011. Using OH LIF or DOAS measurements made no difference in the OH budget analysis which is consistent with previous experiments in SAPHIR where excellent agreement of the two OH detection techniques was demonstrated under various experimental conditions (Schlosser et al., 2007, 2009; Fuchs et al., 2012).

The agreement between P_{OH} and D_{OH} was slightly better at high NO concentrations. However, this difference should be treated with caution considering the experimental uncertainties and the fact that OH destruction and production rates were greater by

ACPD
14, 5535–5560, 2014

a factor of about four under high-NO conditions, mainly caused by greater OH and NO concentrations. Nevertheless, these small differences are consistent with additional OH recycling via $HO_2 + RO_2$ reactions that gain importance under low-NO conditions. Such radical-radical reactions that are usually thought to produce non-radical products can lead to enhanced OH recycling as shown by recent laboratory studies for reactions of carbonyl-containing RO_2 radicals with HO_2 (Hasson et al., 2004; Jenkin et al., 2007; Dillon and Crowley, 2008) and more recently also for the reaction of HO_2 with bicyclic peroxy radicals from aromatic precursors (Birdsall et al., 2010; Birdsall and Elrod, 2011). The influence of the $HO_2 + RO_2$ reactions could only roughly be quantified here in P^*_{OH} by using the measured total RO_2 concentrations and an estimated rate constant from the literature. Despite these uncertainties the small effects were found to have the right magnitude and to go in the right direction. Our data are therefore not in contradiction with the proposed additional OH recycling but cannot confirm it quantitatively. In any case, $RO_2 + HO_2$ reactions played a minor role for the OH budget even under the low-NO conditions of this work.

Current explicit degradation schemes of the Master Chemical Mechanism (MCMv3.2) underestimated OH radical concentrations in previous environmental chamber studies of aromatic compounds (Bloss et al., 2005a, b). This mismatch between simulated OH concentrations and those indirectly inferred from the decay rates of aromatic reactants was attributed to potentially missing OH production processes (Wagner et al., 2003). Our straightforward experimental investigation of the radical balance, however suggests that so far unaccounted OH production reactions are no likely reason for this OH underprediction. Rather there seems to be an overestimation of OH reactivities of secondary products and an underestimation of peroxy radical concentrations in these model simulations as will be discussed in more detail in a companion publication (Nehr et al., 2014).

The high and low NO concentrations employed in this work roughly corresponded to the conditions encountered in the Pearl River Delta field study during morning and afternoon hours, respectively (Hofzumahaus et al., 2009). While in the field campaign

ACPD
14, 5535–5560, 2014

a strong mismatch between OH production and destruction rates by a factor of three was obtained for low-NO conditions, only an insignificant difference was observed here as discussed above. This clearly shows that the presence of aromatic compounds plays no role for the explanation of these field observations.

5 Conclusions

OH production and destruction rates, exclusively calculated from measured quantities, were determined for the first time during SAPHIR atmosphere simulation chamber experiments with the aromatic hydrocarbons benzene, toluene, *p*-xylene and 1,3,5-trimethylbenzene. A widely model-independent, steady-state approach for OH was used for an OH budget determination. Considering primary OH production and recycling reactions by photolysis and HO_2 + NO, measured OH destruction rates slightly exceeded OH production rates by factors ranging between 1.2 and 1.6 under low-NO conditions (0.1–0.2 ppb of NO) and 0.9–1.2 under high-NO conditions (7–8 ppb of NO). CO reference experiments show that the OH budgets were balanced within the accuracy of this analysis. Further OH production in $RO_2 + HO_2$ reactions that have recently been proposed in the literature may be operative but turned out to be insignificant within experimental error under the conditions of this work.

Appendix A

Correction of HO_2 measurement interferences

HO_2-LIF measurements, $[HO_2^*]$, have to be corrected for the concentration of a number of interfering RO_2 radicals, $[RO_2]_i$, detected with the corresponding relative sensitivities

ACPD
14, 5535–5560, 2014

$\alpha^{i}_{RO_2}$ to obtain the true HO_2 concentration, $[HO_2]$ (Fuchs et al., 2011; Lu et al., 2012).

$$[HO_2] = [HO_2{}^*] - \sum_i \alpha^{i}_{RO_2}[RO_2]_i \quad \text{(A1)}$$

Accordingly, the true RO_2 concentration, $[RO_2]$, is given by the sum of the RO_2 concentration measured by LIF, $[RO_2^*]$, plus the contribution of a number of RO_2 radicals, $\alpha^{i}_{RO_2} \times [RO_2]_i$, that was spuriously detected as HO_2.

$$[RO_2] = [RO_2{}^*] + \sum_i \alpha^{i}_{RO_2}[RO_2]_i \quad \text{(A2)}$$

For the correction of the LIF data it was assumed that only RO_2 were detectable by LIF that, after reaction with NO, rapidly form HO_2 by fast fragmentation and/or fast O_2 reaction. For example, in the case of benzene, a significant fraction of secondarily formed peroxy radicals was converted to HO_2 in the detection cell of the LIF instrument (Nehr et al., 2011). Relative detection sensitivities compared to that for HO_2 of $\alpha^{benzene}_{RO_2} = 0.86$ were determined experimentally in 2010. In 2011, $\alpha^{benzene}_{RO_2}$ was then reduced to 0.17 by means of technical changes of the experimental setup (Fuchs et al., 2011). Speciated RO_2 measurements were not available and consequently, the correction of the LIF data was made on the basis of numerical MCMv3.2 simulations. More details on these simulations are given elsewhere (Nehr et al., 2014). Individual organic peroxy radical concentrations, $[RO_2]_i$, were calculated for each SAPHIR experiment. Organic peroxy radicals involved in the photo-oxidation of aromatics and detectable by LIF are listed in Table A1. $\alpha^{benzene}_{RO_2}$ was used for the corrections according to Eqs. A1 and A2 for all $[RO_2]_i$. Additional MCMv3.2 based factors c^{i}_{RO} and $c^{i}_{HO_2}$ that account for the yields of RO in Reaction (R7) and the yields of HO_2 in Reaction (R8), respectively were also considered. Regarding the P_{OH}–D_{OH} relationships the corrections of HO_2 concentrations finally led to ratios D_{OH}/P_{OH} that were greater by 0.17 ± 0.12 for the 2010 data and by 0.05 ± 0.03 for the 2011 data.

ACPD
14, 5535–5560, 2014

Acknowledgements. The authors cordially thank M. Bachner, F. Holland, K. D. Lu, P. Müsgen, and M. Vietz for additional measurements and technical support. B. Bohn and S. Nehr thank the Deutsche Forschungsgemeinschaft for funding under grant BO 1580/3-1.

The service charges for this open access publication have been covered by a Research Centre of the Helmholtz Association.

References

Arneth, A., Schurgers, G., Lathiere, J., Duhl, T., Beerling, D. J., Hewitt, C. N., Martin, M., and Guenther, A.: Global terrestrial isoprene emission models: sensitivity to variability in climate and vegetation, Atmos. Chem. Phys., 11, 8037–8052, doi:10.5194/acp-11-8037-2011, 2011. 5536

Birdsall, A. W. and Elrod, M. J.: Comprehensive NO-dependent study of the products of the oxidation of atmospherically relevant aromatic compounds, J. Phys. Chem. A, 115, 5397–5407, doi:10.1021/jp2010327, 2011. 5539, 5546

Birdsall, A. W., Andreoni, J. F., and Elrod, M. J.: Investigation of the role of bicyclic peroxy radicals in the oxidation mechanism of toluene, J. Phys. Chem. A, 114, 10655–10663, doi:10.1021/jp105467e, 2010. 5539, 5544, 5546

Bloss, C., Wagner, V., Bonzanini, A., Jenkin, M. E., Wirtz, K., Martin-Reviejo, M., and Pilling, M. J.: Evaluation of detailed aromatic mechanisms (MCMv3 and MCMv3.1) against environmental chamber data, Atmos. Chem. Phys., 5, 623–639, doi:10.5194/acp-5-623-2005, 2005a. 5539, 5546

Bloss, C., Wagner, V., Jenkin, M. E., Volkamer, R., Bloss, W. J., Lee, J. D., Heard, D. E., Wirtz, K., Martin-Reviejo, M., Rea, G., Wenger, J. C., and Pilling, M. J.: Development of a detailed chemical mechanism (MCMv3.1) for the atmospheric oxidation of aromatic hydrocarbons, Atmos. Chem. Phys., 5, 641–664, doi:10.5194/acp-5-641-2005, 2005b. 5546

Bohn, B. and Zilken, H.: Model-aided radiometric determination of photolysis frequencies in a sunlit atmosphere simulation chamber, Atmos. Chem. Phys., 5, 191–206, doi:10.5194/acp-5-191-2005, 2005. 5539

ACPD

14, 5535–5560, 2014

Calpini, B., Jeanneret, F., Bourqui, M., Clappier, A., Vajtai, R., and van den Bergh, H.: Direct measurement of the total reaction rate of OH in the atmosphere, Analusis, 27, 328–336, doi:10.1051/analusis:1999270328, 1999. 5540

Calvert, J. G., Atkinson, R., Becker, K.-H., Kamens, R. M., Seinfeld, J. H., Wallington, T. J., and Yarwood, G.: Mechanisms of Atmospheric Oxidation of Aromatic Hydrocarbons, Oxford University Press, New York, USA, 2002. 5545

Crounse, J. D., Paulot, F., Kjaergaard, H. G., and Wennberg, P. O.: Peroxy radical isomerization in the oxidation of isoprene, Phys. Chem. Chem. Phys., 13, 13607–13613, doi:10.1039/C1CP21330J, 2011. 5538

Dillon, T. J. and Crowley, J. N.: Direct detection of OH formation in the reactions of HO_2 with $CH_3C(O)O_2$ and other substituted peroxy radicals, Atmos. Chem. Phys., 8, 4877–4889, doi:10.5194/acp-8-4877-2008, 2008. 5546

Dorn, H., Brandenburger, U., Brauers, T., and Hausmann, H.: A new in-situ laser long-path absorption instrument for the measurement of tropospheric OH radicals, J. Atmos. Sci., 52, 3373–3380, 1995. 5540

Dorn, H.-P., Apodaca, R. L., Ball, S. M., Brauers, T., Brown, S. S., Crowley, J. N., Dubé, W. P., Fuchs, H., Häseler, R., Heitmann, U., Jones, R. L., Kiendler-Scharr, A., Labazan, I., Langridge, J. M., Meinen, J., Mentel, T. F., Platt, U., Pöhler, D., Rohrer, F., Ruth, A. A., Schlosser, E., Schuster, G., Shillings, A. J. L., Simpson, W. R., Thieser, J., Tillmann, R., Varma, R., Venables, D. S., and Wahner, A.: Intercomparison of NO_3 radical detection instruments in the atmosphere simulation chamber SAPHIR, Atmos. Meas. Tech., 6, 1111–1140, doi:10.5194/amt-6-1111-2013, 2013. 5540

Ehhalt, D. H.: Photooxidation of trace gases in the troposphere, Phys. Chem. Chem. Phys., 1, 5401–5408, doi:10.1039/A905097C, 1999. 5537

Finlayson-Pitts, B. J. and Pitts, J. N.: Chemistry of the Upper and Lower Atmosphere: Theory, Experiments, and Applications, Academic Press, San Diego, USA, 2000. 5537

Fortin, T. J., Howard, B. J., Parrish, D. D., Goldan, P. D., Kuster, W. C., Atlas, E. L., and Harley, R. A.: Temporal changes in US benzene emissions inferred from atmospheric measurements, Environ. Sci. Technol., 39, 1403–1408, doi:10.1021/es049316n, 2005. 5537

Fuchs, H., Holland, F., and Hofzumahaus, A.: Measurement of tropospheric RO_2 and HO_2 radicals by a laser-induced fluorescence instrument, Rev. Sci. Instrum., 79, 084104, doi:10.1063/1.2968712, 2008. 5540

ACPD
14, 5535–5560, 2014

Fuchs, H., Ball, S. M., Bohn, B., Brauers, T., Cohen, R. C., Dorn, H.-P., Dubé, W. P., Fry, J. L., Häseler, R., Heitmann, U., Jones, R. L., Kleffmann, J., Mentel, T. F., Müsgen, P., Rohrer, F., Rollins, A. W., Ruth, A. A., Kiendler-Scharr, A., Schlosser, E., Shillings, A. J. L., Tillmann, R., Varma, R. M., Venables, D. S., Villena Tapia, G., Wahner, A., Wegener, R., Wooldridge, P. J., and Brown, S. S.: Intercomparison of measurements of NO_2 concentrations in the atmosphere simulation chamber SAPHIR during the NO3Comp campaign, Atmos. Meas. Tech., 3, 21–37, doi:10.5194/amt-3-21-2010, 2010. 5540

Fuchs, H., Bohn, B., Hofzumahaus, A., Holland, F., Lu, K. D., Nehr, S., Rohrer, F., and Wahner, A.: Detection of HO_2 by laser-induced fluorescence: calibration and interferences from RO_2 radicals, Atmos. Meas. Tech., 4, 1209–1225, doi:10.5194/amt-4-1209-2011, 2011. 5540, 5543, 5548

Fuchs, H., Dorn, H.-P., Bachner, M., Bohn, B., Brauers, T., Gomm, S., Hofzumahaus, A., Holland, F., Nehr, S., Rohrer, F., Tillmann, R., and Wahner, A.: Comparison of OH concentration measurements by DOAS and LIF during SAPHIR chamber experiments at high OH reactivity and low NO concentration, Atmos. Meas. Tech., 5, 1611–1626, doi:10.5194/amt-5-1611-2012, 2012. 5540, 5545

Fuchs, H., Hofzumahaus, A., Rohrer, F., Bohn, B., Brauers, T., Dorn, H.-P., Haeseler, R., Holland, F., Kaminski, M., Li, X., Lu, K., Nehr, S., Tillmann, R., Wegener, R., and Wahner, A.: Experimental evidence for efficient hydroxyl radical regeneration in isoprene oxidation, Nat. Geosci., 6, 1023–1026, doi:10.1038/NGEO1964, 2013. 5538, 5540

Hasson, A. S., Tyndall, G. S., and Orlando, J. J.: A product yield study of the reaction of HO_2 radicals with ethyl peroxy ($C_2H_5O_2$), acetyl peroxy ($CH_3C(O)O_2$), and acetonyl peroxy ($CH_3C(O)CH_2O_2$) radicals, J. Phys. Chem. A, 108, 5979–5989, doi:10.1021/jp048873t, 2004. 5546

Hawthorne, S., Miller, D., Barkley, R., and Krieger, M.: Identification of methoxylated phenols as candidate tracers for atmospheric wood smoke pollution, Environ. Sci. Technol., 22, 1191–1196, 1988. 5537

Hofzumahaus, A., Rohrer, F., Lu, K., Bohn, B., Brauers, T., Chang, C.-C., Fuchs, H., Holland, F., Kita, K., Kondo, Y., Li, X., Lou, S., Shao, M., Zeng, L., Wahner, A., and Zhang, Y.: Amplified trace gas removal in the troposphere, Science, 324, 1702–1704, doi:10.1126/science.1164566, 2009. 5538, 5540, 5546

ACPD
14, 5535–5560, 2014

Holland, F., Hofzumahaus, A., Schäfer, R., Kraus, A., and Pätz, H.-W.: Measurements of OH and HO_2 radical concentrations and photolysis frequencies during BERLIOZ, J. Geophys. Res.-Atmos., 108, 8246–8268, doi:10.1029/2001JD001393, 2003. 5540

IUPAC: Subcommittee for Gas Kinetic Data Evaluation, available at: http://iupac.pole-ether.fr/ (last access: 11 October 2013), 2013. 5542

Jenkin, M. E., Hurley, M. D., and Wallington, T. J.: Investigation of the radical product channel of the $CH_3C(O)O_2 + HO_2$ reaction in the gas phase, Phys. Chem. Chem. Phys., 9, 3149–3162, doi:10.1039/B702757E, 2007. 5546

Johnson, M. M., Williams, R., Fan, Z., Lin, L., Hudgens, E., Gallagher, J., Vette, A., Neas, L., and Ozkaynak, H.: Participant-based monitoring of indoor and outdoor nitrogen dioxide, volatile organic compounds, and polycyclic aromatic hydrocarbons among MICA-Air households, Atmos. Environ., 44, 4927–4936, doi:10.1016/j.atmosenv.2010.08.027, 2010. 5537

Karl, M., Brauers, T., Dorn, H.-P., Holland, F., Komenda, M., Poppe, D., Rohrer, F., Rupp, L., Schaub, A., and Wahner, A.: Kinetic study of the OH-isoprene and O_3-isoprene reaction in the atmosphere simulation chamber, SAPHIR, Geophys. Res. Lett., 31, L05117, doi:10.1029/2003GL019189, 2004. 5539

Kleffmann, J.: Daytime sources of nitrous acid (HONO) in the atmospheric boundary layer, ChemPhysChem, 8, 1137–1144, doi:10.1002/cphc.200700016, 2007. 5537

Lelieveld, J., Butler, T. M., Crowley, J. N., Dillon, T. J., Fischer, H., Ganzeveld, L., Harder, H., Lawrence, M. G., Martinez, M., Taraborrelli, D., and Williams, J.: Atmospheric oxidation capacity sustained by a tropical forest, Nature, 452, 737–740, doi:10.1038/nature06870, 2008. 5538

Lou, S., Holland, F., Rohrer, F., Lu, K., Bohn, B., Brauers, T., Chang, C.C., Fuchs, H., Häseler, R., Kita, K., Kondo, Y., Li, X., Shao, M., Zeng, L., Wahner, A., Zhang, Y., Wang, W., and Hofzumahaus, A.: Atmospheric OH reactivities in the Pearl River Delta – China in summer 2006: measurement and model results, Atmos. Chem. Phys., 10, 11243–11260, doi:10.5194/acp-10-11243-2010, 2010. 5539, 5540

Lu, K. D., Rohrer, F., Holland, F., Fuchs, H., Bohn, B., Brauers, T., Chang, C. C., Häseler, R., Hu, M., Kita, K., Kondo, Y., Li, X., Lou, S. R., Nehr, S., Shao, M., Zeng, L. M., Wahner, A., Zhang, Y. H., and Hofzumahaus, A.: Observation and modelling of OH and HO_2 concentrations in the Pearl River Delta 2006: a missing OH source in a VOC rich atmosphere, Atmos. Chem. Phys., 12, 1541–1569, doi:10.5194/acp-12-1541-2012, 2012. 5538, 5548

ACPD
14, 5535–5560, 2014

Nehr, S., Bohn, B., Fuchs, H., Hofzumahaus, A., and Wahner, A.: HO_2 formation from the OH plus benzene reaction in the presence of O_2, Phys. Chem. Chem. Phys., 13, 10699–10708, doi:10.1039/C1CP20334G, 2011. 5539, 5543, 5548

Nehr, S., Bohn, B., and Wahner, A.: Prompt HO_2 formation following the reaction of OH with aromatic compounds under atmospheric conditions, J. Phys. Chem. A, 116, 6015–6026, doi:10.1021/jp210946y, 2012. 5539

Nehr, S., Bohn, B., Brauers, T., Dorn, H.-P., Fuchs, H., Häseler, R., Hofzumahaus, A., Li, X., Lu, K. D., Rohrer, F., Tillmann, R., and Wahner, A.: Atmospheric photochemistry of aromatic hydrocarbons: validation of MCMv3.2 against SAPHIR chamber data, Atmos. Chem. Phys. Discuss., in preparation, 2014. 5546, 5548

Niedojadlo, A., Becker, K.-H., Kurtenbach, R., and Wiesen, P.: The contribution of traffic and solvent use to the total NMVOC emission in a German city derived from measurements and CMB modelling, Atmos. Environ., 41, 7108–7126, doi:10.1016/j.atmosenv.2007.04.056, 2007. 5537

Peeters, J., Nguyen, T. L., and Vereecken, L.: HO_x radical regeneration in the oxidation of isoprene, Phys. Chem. Chem. Phys., 11, 5935–5939, doi:10.1039/B908511D, 2009. 5538

Piccot, S. D., Watson, J. J., and Jones, J. W.: A global inventory of volatile organic compound emissions from anthropogenic sources, J. Geophys. Res.-Atmos., 97, 9897–9912, doi:10.1029/92JD00682, 1992. 5536

Poppe, D., Brauers, T., Dorn, H.-P., Karl, M., Mentel, T. F., Schlosser, E., Tillmann, R., Wegener, R., and Wahner, A.: OH-initiated degradation of several hydrocarbons in the atmosphere simulation chamber SAPHIR, J. Atmos. Chem., 57, 203–214, doi:10.1007/s10874-007-9065-y, 2007. 5539

Rohrer, F., Bohn, B., Brauers, T., Brüning, D., Johnen, F.-J., Wahner, A., and Kleffmann, J.: Characterisation of the photolytic HONO-source in the atmosphere simulation chamber SAPHIR, Atmos. Chem. Phys., 5, 2189–2201, doi:10.5194/acp-5-2189-2005, 2005. 5537, 5541, 5543

Sadanaga, Y., Yoshino, A., Watanabe, K., Yoshioka, A., Wakazono, Y., Kanaya, Y., and Kajii, Y.: Development of a measurement system of OH reactivity in the atmosphere by using a laser-induced pump and probe technique, Rev. Sci. Instrum., 75, 2648–2655, doi:10.1063/1.1775311, 2004. 5540

Schlosser, E., Bohn, B., Brauers, T., Dorn, H.-P., Fuchs, H., Häseler, R., Hofzumahaus, A., Holland, F., Rohrer, F., Rupp, L. O., Siese, M., Tillmann, R., and Wahner, A.: Intercompari-

ACPD
14, 5535–5560, 2014

son of two hydroxyl radical measurement techniques at the atmosphere simulation chamber SAPHIR, J. Atmos. Chem., 56, 187–205, doi:10.1007/s10874-006-9049-3, 2007. 5540, 5545

Schlosser, E., Brauers, T., Dorn, H.-P., Fuchs, H., Häseler, R., Hofzumahaus, A., Holland, F., Wahner, A., Kanaya, Y., Kajii, Y., Miyamoto, K., Nishida, S., Watanabe, K., Yoshino, A., Kubistin, D., Martinez, M., Rudolf, M., Harder, H., Berresheim, H., Elste, T., Plass-Dülmer, C., Stange, G., and Schurath, U.: Technical Note: Formal blind intercomparison of OH measurements: results from the international campaign HOxComp, Atmos. Chem. Phys., 9, 7923–7948, doi:10.5194/acp-9-7923-2009, 2009. 5540, 5545

Wagner, V., Jenkin, M. E., Saunders, S. M., Stanton, J., Wirtz, K, and Pilling, M. J.: Modelling of the photooxidation of toluene: conceptual ideas for validating detailed mechanisms, Atmos. Chem. Phys., 3, 89–106, doi:10.5194/acp-3-89-2003, 2003. 5546

Wegener, R., Brauers, T., Koppmann, R., Rodrigues-Bares, S., Rohrer, F., Tillmann, R., Wahner, A., Hansel, A., and Wisthaler, A.: Simulation chamber investigation of the reactions of ozone with short-chained alkenes, J. Geophys. Res.-Atmos., 112, D13301, doi:10.1029/2006JD007531, 2007. 5540

Wolfe, G. M., Crounse, J. D., Parrish, J. D., St. Clair, J. M., Beaver, M. R., Paulot, F., Yoon, T. P., Wennberg, P. O., and Keutsch, F. N.: Photolysis, OH reactivity and ozone reactivity of a proxy for isoprene-derived hydroperoxyenals (HPALDs), Phys. Chem. Chem. Phys., 14, 7276–7286, doi:10.1039/C2CP40388A, 2012. 5538

ACPD
14, 5535–5560, 2014

Table 1. Properties of key instruments for the investigation of OH budgets during SAPHIR experiments.

observable	method	time resolution/s	1σ precision	accuracy/ %
OH	Laser-induced fluorescence (LIF)	47	0.3×10^6 cm^{-3}	10
HO_2, RO_2	Laser-induced fluorescence (LIF)	47	1×10^7 cm^{-3}	10*
OH	Differential optical absorption spectroscopy (DOAS)	205	0.8×10^6 cm^{-3}	6.5
k_{OH}	Flash photolysis/Laser-induced fluorescence (FP/LIF)	180	0.3 s^{-1}	5
NO	Chemiluminescence (CL)	90	0.005 ppb	7

* RO_2 interference effects not included, see text.

ACPD
14, 5535–5560, 2014

Table 2. Compilation of SAPHIR experiments with starting concentrations of aromatic hydrocarbons ([aromatic]$_0$). These concentrations were calculated from the initial increase of k_{OH} upon addition of reactants using OH rate constants from MCMv3.2. [NO]$_{max}$ denotes peak NO concentration during the experiments.

date	[aromatic]$_0$/ppb	[NO]$_{max}$/ppb
benzene		
07 Jun 2010[b]	230	0.75
23 Jun 2010	235	0.55
01 Aug 2011	250	0.20
08 Jun 2010[b]	235	7.6[a]
25 Jun 2010	215	7.6[a]
toluene		
05 Jul 2010[b]	65	0.46
04 Aug 2011	107	0.27
13 Jun 2010	60	7.1[a]
p-xylene		
14 Jun 2010	26	0.35
02 Jul 2010	26	0.35
07 Aug 2011	29	0.35
16 Jun 2010	24	6.9[a]
30 Jun 2010	24	7.1[a]
1,3,5-TMB		
17 Jun 2010	6.0	0.48
01 Jul 2010	6.5	0.45
10 Aug 2011	7.2	0.26
21 Jun 2010[b]	6.0	7.2[a]
28 Jun 2010	6.5	7.6[a]

[a] High NO experiment.
[b] No HONO measurements available.

ACPD
14, 5535–5560, 2014

Table 3. Analysis of OH budgets during SAPHIR experiments. Means and standard deviations of the ratios P_{OH}/D_{OH} and P^*_{OH}/D_{OH} calculated from measurements according to Eqs. (2) and (5), respectively. The data evaluation was restricted to time periods where the chamber was illuminated and aromatic OH reactants were present. *N* denotes the number of data points.

date	*N*	D_{OH}/P_{OH}	D_{OH}/P^*_{OH}
benzene			
07 Jun 2010	98	1.34 ± 0.32	1.28 ± 0.29
23 Jun 2010	118	1.32 ± 0.37	1.22 ± 0.33
01 Aug 2011	51	1.48 ± 0.31	1.44 ± 0.29
08 Jun 2010*	105	0.92 ± 0.22	0.91 ± 0.22
25 Jun 2010*	101	0.92 ± 0.60	0.90 ± 0.56
toluene			
05 Jul 2010	107	1.42 ± 0.29	1.14 ± 0.22
04 Aug 2011	35	1.56 ± 0.68	1.37 ± 0.49
13 Jun 2010*	53	1.17 ± 0.34	1.01 ± 0.20
p-xylene			
14 Jun 2010	71	1.60 ± 0.35	1.29 ± 0.29
02 Jul 2010	78	1.52 ± 0.37	1.09 ± 0.25
07 Aug 2011	15	1.59 ± 0.61	1.44 ± 0.51
16 Jun 2010*	53	1.12 ± 0.31	1.01 ± 0.20
30 Jun 2010*	50	1.05 ± 0.47	0.89 ± 0.17
1,3,5-TMB			
17 Jun 2010	68	1.23 ± 0.26	1.07 ± 0.18
01 Jul 2010	52	1.09 ± 0.18	0.69 ± 0.13
10 Aug 2011	41	1.30 ± 0.40	1.02 ± 0.20
21 Jun 2010*	67	1.04 ± 0.22	1.01 ± 0.19
28 Jun 2010*	12	1.11 ± 0.11	0.99 ± 0.10

* High-NO experiment.

ACPD
14, 5535–5560, 2014

Table A1. Organic peroxy radicals (MCM specific designation) detectable by LIF and their respective RO yields (c_{RO}) in $RO_2 + NO$ reactions and subsequent HO_2 yields (c_{HO_2}) in $RO + O_2$ reactions as implemented in MCMv3.2.

RO_2 species	benzene	toluene	*p*-xylene	1,3,5-TMB	c_{RO}	c_{HO_2}
BZBIPERO2	×				0.92	1.00
BZEMUCO2	×				0.90	0.50
C5DIALO2	×				1.00	1.00
PHENO2	×				1.00	1.00
HCOCO3	×	×	×	×	1.00	1.00
HOCH2CO3	×	×	×	×	1.00	1.00
MALDIALCO3	×	×			1.00	1.00
C3DIALO2	×	×			1.00	1.00
MALDIALO2	×	×			1.00	1.00
NBZFUO2	×	×			1.00	0.50
BZFUO2	×	×			1.00	1.00
HCOCOHCO3	×	×	×		1.00	1.00
NCATECO2	×				1.00	1.00
C5CO2OHCO3	×				1.00	1.00
C4CO2DBCO3	×				1.00	1.00
C6H5CH2O2		×			0.90	1.00
TLBIPERO2		×			0.89	1.00
CRESO2		×			1.00	1.00
TLEMUCO2		×			0.90	0.50
C615CO2O2		×			1.00	1.00
C5CO14O2		×	×		1.00	0.17
C3MCODBCO3		×	×		1.00	1.00
MC3CODBCO3		×	×		1.00	0.65
C4M2ALOHO2		×	×		1.00	1.00
C5DICARBO2		×			1.00	1.00
TLFUO2		×			1.00	1.00
MNCATECO2		×			1.00	1.00
PXYFUO2		×			1.00	1.00
CO2H3CO3		×	×	×	1.00	1.00
C6CO2OHCO3		×			1.00	1.00
PXYLO2			×		0.90	1.00
PXYBIPERO2			×		0.86	1.00
PXYMUCO2			×		0.83	0.50
C6M5CO2O2			×		1.00	1.00
PXYOLO2			×		1.00	1.00
C3MDIALO2			×	×	1.00	1.00
DMKOHO2			×		1.00	0.30
PXYFUO2			×		1.00	1.00
C4CO2O2			×		1.00	0.50
CHOMOHCO3			×	×	1.00	1.00
PXNCATECO2			×		1.00	1.00
TL4OHNO2O2			×		1.00	1.00
C6MOHCOCO3			×		1.00	1.00
C5DBCO2CO3			×		1.00	1.00
TMBO2				×	0.90	1.00
TM135BPRO2				×	0.84	1.00
TM135OLO2				×	1.00	1.00
TM135MUCO2				×	0.94	0.50
C5MCO2OHO2				×	1.00	1.00
MXYFUO2				×	1.00	1.00
C4COMOHCO3				×	1.00	1.00

ACPD
14, 5535–5560, 2014

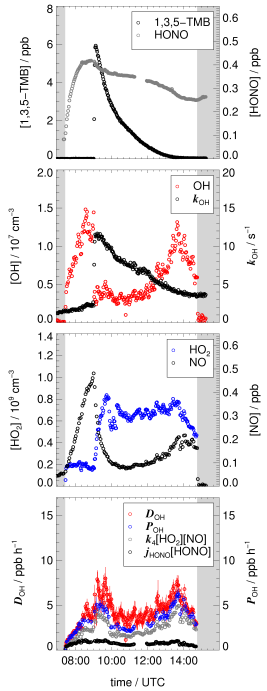

Fig. 1. Measurements of selected quantities performed during a low-NO SAPHIR experiment with 1,3,5-TMB on 17 June 2010. Grey shaded areas indicate time periods when the chamber roof was closed. Formation of HONO, the major OH precursor in SAPHIR, was observed by LOPAP just after the humidified chamber was exposed to sunlight (grey points, upper panel). The injection of 1,3,5-TMB was observed by PTR-TOF-MS (upper panel) and the OH reactivity instrument (k_{OH}, second panel). OH and NO rapidly decreased whereas HO_2 increased after the 1,3,5-TMB addition (middle panels). Diurnal profiles of P_{OH} and D_{OH} (lower panel) were calculated according to Eqs. (2) and (3). Other data in the lower panel show the main terms contributing to P_{OH}.

ACPD
14, 5535–5560, 2014

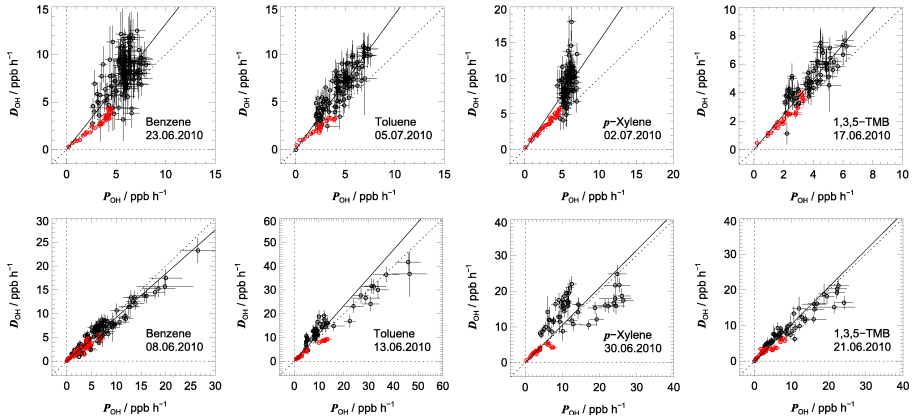

Fig. 2. Correlation of OH destruction rates (D_{OH}) and production rates (P_{OH}) for SAPHIR experiments in 2010 under low-NO conditions (upper panels) and high-NO conditions (lower panels). Black and red data points indicate different periods of the experiments. Red: zero air period; Black: after the injection of aromatics. The solid lines correspond to the mean ratios listed in the third column of Table 3 (P_{OH} calculated by Eq. 2), dashed lines are 1 : 1 lines.

ACPD
14, 5535–5560, 2014